A Numerical Simulator of Ocean Internal Waves for Long-Range Acoustics

by Frank S. Henyey and Stephen A. Reynolds

Technical Memoradum
APL-UW TM 1-13
March 2013

Applied Physics Laboratory University of Washington
1013 NE 40th Street Seattle, Washington 98105-6698

Grant N00014-1-31-0009

ACKNOWLEDGMENTS

We thank the Office of Naval Research for earlier support that led to this simulator, and the Applied Physics Laboratory at the University of Washington for support while completing this report. Rex Andrew edited this report, with support from ONR grant N00014-1-31-0009.

ABSTRACT

In combination with an appropriate background ocean model, simulations of internal waves are necessary to create realistic scenarios for use in acoustic propagation studies. Our approach employs contemporary understanding of internal wave statistics with a simulator that produces two-dimensional (range/depth) slices of internal wave displacements. The method produces statistical realizations for acoustic studies that are true to ocean measurements with nominal computational cost.

This page is blank intentionally.

1 Introduction

This report describes a numerical simulator that produces realizations of internal wave displacements for use in studies of long-range acoustic propagation. The goals of any simulator are twofold: first to produce simulations that are realistic, and second, to do so efficiently.

There are a variety of numerical simulators for internal waves. Like the one described here, most are spectral models. These models commonly utilize the formulation for the Garrett and Munk (GM) spectrum and in particular, the formulation based on a simplified Wentzel–Kramers–Brillouin (WKB) approximation [6]. In shallow water or near the surface, these WKB approximations are not valid. Taking a non-WKB approach improves simulation realism with little cost, and provides an algorithm valid in both deep and shallow water.

For several years, the simulator described as a starting field in Winters and D'Asaro [7] (hereinafter WD97) was employed to model situations involving relatively short-range acoustic transmission experiments, i.e., less than 50 km. The fields may be incremented in time consistent with the internal wave dispersion relationship and the method is almost free of the WKB limitation. For shallow water and short-range situations, their approach was extended to relax this limitation. However, because the code is three-dimensional, the approach is computationally intensive. And, to minimize memory usage, strict limits are imposed on the smallest and largest wave numbers that may be represented.

An attempt was made to use 3-D fields from the WD97 technique for long-range propagation studies. Two-dimensional depth-range fields were obtained by slicing through the 3-D field along an angle, then interpolating the field onto the desired grid. This allows continuous slices to any range to be formed. In WD97, 2-D horizontal fast Fourier transforms (FFTs) are taken at each depth so the fields are periodic about the boundaries. Unfortunately, periodicities related to the size of the box inevitably are produced in the output fields. So WD97 produces reasonably realistic fields within its domain. However, it is computationally intensive and when extended to long range, the resulting fields are not realistic. The WD97 approach was not designed for long-range propagation studies.

It was realized that by sampling in k_x and $k = \sqrt{k_x^2 + k_y^2}$ rather than the traditional k_x and k_y, only a moderate number of k-values are required. But a trade-off is made: the problem reduces to a single Fourier transform in x providing a field at one (or a few) y-values. The resulting internal wave simulator is very efficient and meets our requirements of producing displacement fields that (1) have megameter or greater periodicities, (2) are not constrained by the WKB approximation, and (3) contain a broad range of vertical and horizontal scales. Hence the simulator generates realistic fields to very long ranges (megameters). In section II, the formulation is described. In section III, examples and results from tests are shown. An appendix presents a pseudo-code for reference by those wishing copies of the software.

2 Method

Much of our formalism develops from Henyey et al. [4] (hereinafter H97). The numerical simulator follows the presentation in WD97, where a general method for a five-variable simulation is presented. Here, obtaining sound speed variations requires only the internal wave displacement field. Depict this field in two dimensions as $\zeta(x, y, z; t)$. The third dimension $y = 0$. Note that throughout this discussion, time is considered a parameter. For convenience consider the displacement field in terms of the component horizontal wave number k_x , where x and k_x are Fourier transform pairs, then

$$\zeta(k_x, y, z) = \int e^{iyk_y} \sum_{j=1}^{M} \{G_- e^{-i\omega_{jk}t} + G_+ e^{i\omega_{jk}t}\} \varphi_{j,k}(z) dk_y \tag{1}$$

which is analogous to Eq. 18 in WD97.

We evaluate this expression at a given $y = y_0$. An inverse Fourier transform at each depth provides $\zeta(x, y_0, z; t)$. In an ocean modeled as horizontally infinite in both directions, G_- and G_+ are generalized functions of a continuous wave vector. From this point we will, as an approximation, treat them as ordinary functions of a discrete wave vector. Each of the discrete wave vectors is representative of a small area of continuous wave vector surrounding the discrete value. These areas fill up the whole space without overlapping. The value of G_- or G_+ at one of the discrete points is the average of the corresponding generalized function over the area surrounding that point.

For a finite depth ocean, there is a decomposition in the wave field in vertical modes $\varphi_{j,k}(z)$, where mode number $j = 1, 2, \ldots, M$. The modes $\varphi_{j,k}(z)$ and their frequencies are functions of the horizontal wave number k, where $k^2 = k_x^2 + k_y^2$ (cf. WD97 Eq. 8 ff.). The modes and frequencies ω_{jk} are obtained by a method that has been passed from researcher to researcher for many years. We map the problem onto finding the eigenvalues and eigenvectors of a symmetric, tri-diagonal matrix. In terms of eigenfunctions $\psi = \sqrt{n^2 - f^2}\varphi$, Eq. 8 of WD97 for the vertical modes may be written as

$$\frac{1}{\sqrt{n^2 - f^2}} (k^2 - \partial_z^2) \frac{1}{\sqrt{n^2 - f^2}} \psi = \lambda \psi \tag{2}$$

The eigenvalues

$$\lambda = k^2/(\omega^2 - f^2) \tag{3}$$

and eigenfunctions are obtained using a tri-diagonal mode solver. In this mapping, the mode normalization

$$\int_{-L_z}^{0} (n^2 - f^2) \varphi_{j,k}(z) \varphi_{j',k}(z)\, dz = \delta_{jj'} \tag{4}$$

and boundary conditions, $\varphi_{j,k}(-L_z) = \varphi_{j,k}(0) = 0$ are preserved.

To obtain the displacement field in two dimensions for a given depth as a function of horizontal wave number, there is a summation over j and over k. This differs from WD97. The reduction to two dimensions requires us to define k_y in terms of k and k_x.

The wave amplitudes are determined by G_- and G_+. These are complex random deviates generated separately to allow independent right- and left-going waves. G_- and G_+ have zero mean, with a variance given by the internal wave spectrum defined below and by the wave number area represented by one wave vector. The variance is proportional to 1/area because of the averaging of delta-correlated quantities.

The technique defined in Eq. 1 is common. Realizations are obtained via Monte Carlo method on the weights, G_- and G_+. A displacement realization is generated in the wave number domain, with amplitude determined by the model spectrum. Note that the depth dependence is specified by the amplitudes of the vertical modes. (This property is one step in freeing us from the WKB approximation.) At this stage, WD97 uses a 2-D inverse Fourier transform at each depth and obtains the field in the 3-D spatial domain.

Our method uses the full spectral model. This is reduced to one dimension in the horizontal by summing over circles or annuli in horizontal wave number space. Once generated in the wave number domain, only a one-dimensional inverse FFT is needed to obtain the field in range. The result is an efficient and accurate algorithm.

Consider the differential displacement variance in frequency, mode number, and horizontal wave number

$$S(\omega, j) d\omega dj \frac{d\theta}{2\pi} \tag{5}$$

Though the mode number increment, dj, equals 1, we leave it in for completeness. We assume the spectrum and the vertical modes are independent of horizontal direction (i.e., the field is horizontally isotropic). In Eq. 5, θ is the direction of the horizontal wave number. Writing the variance in terms of increments in horizontal wave numbers gives

$$S(\omega, j) d\omega dj \frac{d\theta}{2\pi} = \frac{S(\omega, j) d\omega}{2\pi k dk} dj dk_x dk_y \tag{6}$$

Recognizing the group speed, $v_g = d\omega/dk$, and folding the k_y integral to the positive k_y side, the differential variance becomes

$$var = \frac{S(\omega, j) v_g}{\pi k} dj dk_x d|k_y| \tag{7}$$

In terms of the annulus $k_i < k < k_f$,

$$dk = k_f - k_i \tag{8}$$

$$d|k_y| = \sqrt{k_f^2 - k_x^2} - \sqrt{k_i^2 - k_x^2} \tag{9}$$

At this point, our derivation has diverged from H97. Finally, using Eq. 6, with $\langle \cdot \rangle$ denoting an expected value,

$$\langle |G_+|^2 \rangle + \langle |G_-|^2 \rangle = \frac{S(\omega, j) v_g}{\pi k} dj dk_x d|k_y| \tag{10}$$

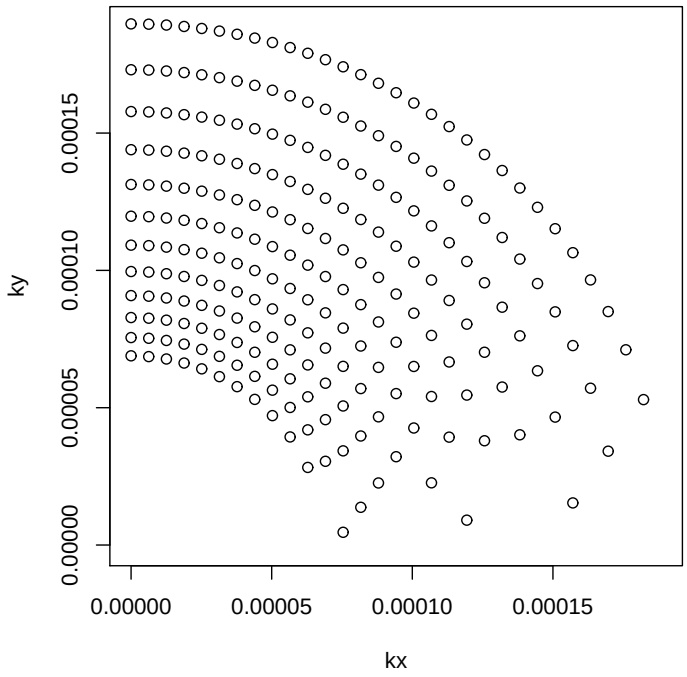

Figure 1: Example of the sampling in the first quadrant of the (k_x, k_y) plane. Only the first 12 values of horizontal wave number k are shown, corresponding to $m = 0, 1, 2, \ldots, 11$. The logarithmic spacing in k is already evident. The gridding is uniform in k_x. Only 12 modes need be computed to support this constellation of sample points in (k_x, k_y) space.

This assumes a two-sided spectrum in k_x. The Jacobian

$$J = \frac{v_g}{\pi k} \tag{11}$$

arises from the conversion of $d\omega d\theta$ to $dk_x d|k_y|$.

Due to horizontal isotropy, the computational effort of calculating the modes can be significantly reduced over that involved in a standard sampling of the (k_x, k_y) plane by only computing the modes on a grid of $k = \sqrt{k_x^2 + k_y^2}$ values. The sampling here is also chosen to have logarithmic spacing with the first increment in each decade equal to about 10% over the first value. This puts about 25 sample points in each decade. Thus, the horizontal wave number spacing is given as $k_m = k_0 r^m$, $m = 0, 1, 2, \ldots$ with $r = 10^{0.04}$. The lowest mode wave number is set as $k_0 = 2\pi/L_{kh0}$, where L_{kh0} is the length scale of this mode.

The conversion from sampling in (k_x, k_y) to sampling in (k, k_x) on annuli of constant k results in non-uniform contributions to the simulation along the k_y axis (Fig. 1). Here, the sample (k_x, k_y) locations for the first 12 "rings" ($m = 0, 1, 2, \ldots, 11$) are shown, and $L_{kh0} = 1 \times 10^5$ m and $\Delta k_x = 2\pi/L_x$ with $L_x = 1 \times 10^6$ m. Only the (k_x, k_y) sample locations corresponding to positive $k_y^2 = k^2 - k_x^2$ are valid. This results in sparse samping near the k_x

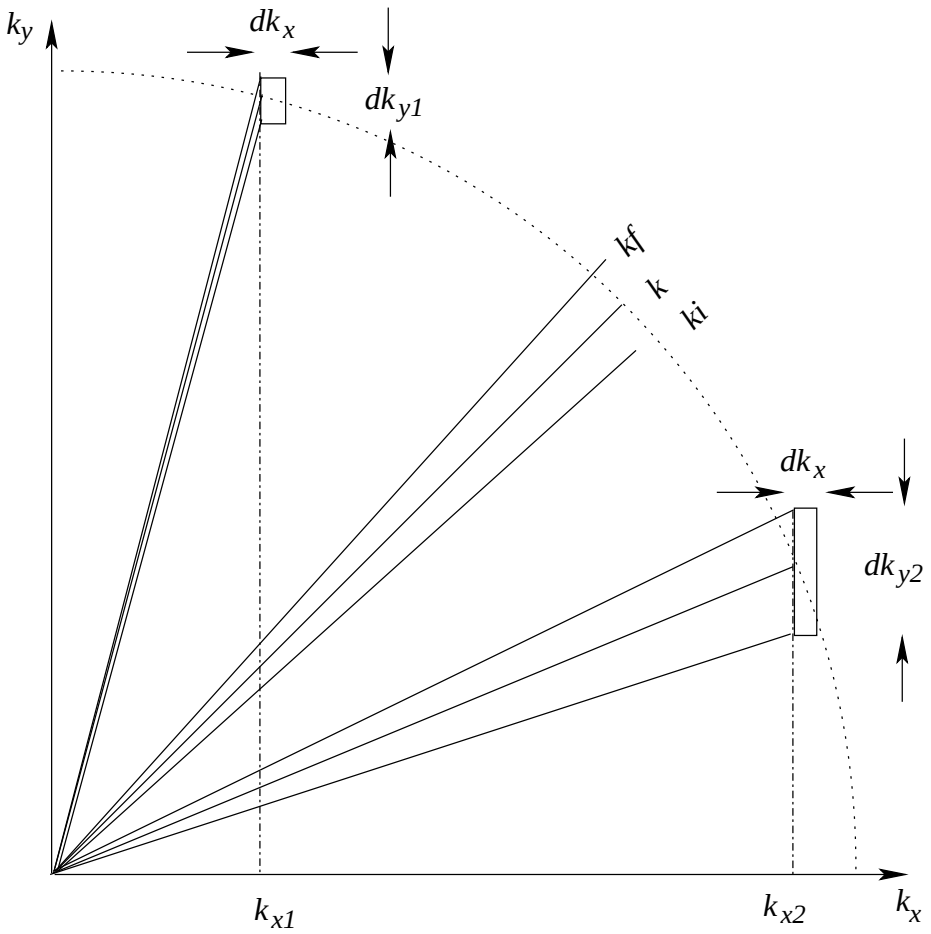

Figure 2: Examples of the differential areal tiling based on the (k, k_x) sampling scheme. The example presents only the sampling in the first quadrant of the (k_x, k_y) plane.

axis. This scheme is designed for accurate simulations along the x axis, but not the y axis.

The differential variance contributions defined by Eq. 9 result in a non-uniform $k_x - k_y$ tiling of the (k_x, k_y) plane (Fig. 2). A small correction to the differential variance contribution (Eq. 9) is required for the first ring, or differential elements adjacent to the k_x axis. If $m = 0$ or $k_i \leq k_x$, then $d|k_y| = \sqrt{k_f^2 - k_x^2}$. This essentially models the contribution as coming from a triangle with an apex at the origin (instead of a rectangle).

The group speed $d\omega/dk$ is obtained directly using the Hellmann–Feynman theorem [2,3].

Using Eq. 3,

$$\frac{d\omega}{dk} = \frac{1}{2}\frac{k}{\omega\lambda}\left[2 - \frac{k}{\lambda}\frac{d\lambda}{dk}\right] \tag{12}$$

The term $d\lambda/dk$ can be computed from Eq. 2. Differentiating both sides of Eq. 2 by k yields

$$\frac{2k}{n^2 - f^2}\psi = \frac{d\lambda}{dk}\psi \tag{13}$$

Multiplying both sides by ψ and integrating over depth yields

$$2k\int \varphi^2(z)\,dz = \frac{d\lambda}{dk}\int (n^2 - f^2)\varphi^2(z)\,dz \tag{14}$$

using the definition of ψ. However, from Eq. 4, $\int (n^2 - f^2)\varphi^2\,dz = 1$. Hence

$$\frac{d\omega}{dk} = \frac{k}{\omega\lambda}\left[1 - \frac{k^2}{\lambda}\int \varphi^2\,dz\right] \tag{15}$$

$$= \frac{\omega^2 - f^2}{\omega k}\left[1 - (\omega^2 - f^2)\int \varphi^2\,dz\right] \tag{16}$$

Thus, once the modes φ and the eigenfrequencies ω have been computed, the group speed $d\omega/dk$ can be determined directly. No WKB approximations are required in this step.

To this point, any spectrum could be used. We follow H97 who utilize a GM spectrum modified so as not to include WKB approximations. This model decomposes into frequency and vertical mode number. In this representation the spectrum is separable. H97 defines the spectrum as

$$S(\omega, j) = (BE_{GM})(n_0 B)^2 H(j)\frac{2}{\pi}\frac{f}{\omega^3}\sqrt{\omega^2 - f^2} \tag{17}$$

where

$$n_0 B = \int n(z)dz \tag{18}$$

and

$$H(j) = \frac{H_0}{j^2 + j_*^2} \tag{19}$$

The constant H_0 normalizes to unity the summation of $H(j)$. The WKB limitation is removed from the traditional GM spectral model. Density does not enter this formulation; the spectrum is in terms of energy per unit mass. Note BE_{GM} is a single parameter and j_* is the traditional characteristic (vertical) mode number. Both BE_{GM} and j_* must be specified in each simulation. GM neglected the contribution of the deeper part of the ocean in the integral of Eq. 18, resulting in a significant underestimate of $n_0 B$. If a corrected value of $n_0 B$ is used, both BE_{GM} and j_* should be appropriately adjusted. Note also that Eq. 1 is written as a function of y. At this time, we have only implemented the code to evaluate the field at a single value of y_0. For convenience, we have selected the plane $y_0 = 0$.

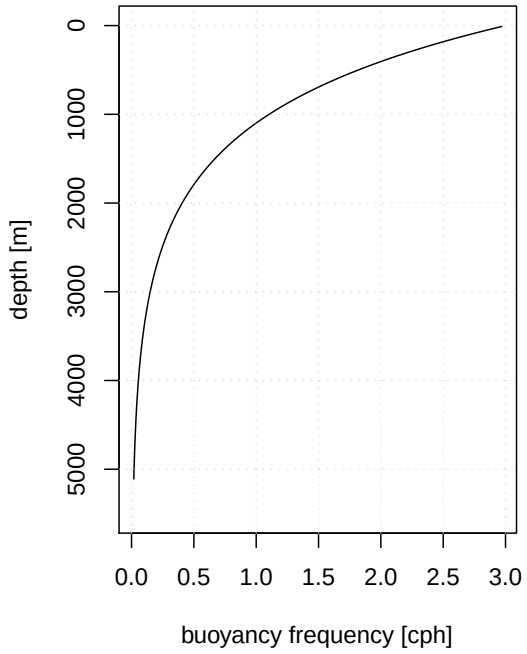

Figure 3: Buoyancy profile used in the tests. The profile is the "Munk canonical profile" modified by the Coriolis frequency at 25°.

3 Tests

We present two tests to demonstrate both the validity and viability of the method. First we examine the variance of the simulated internal wave variability. The second explores the distribution of energy in horizontal wave number. In both cases, the numerical results are compared with predictions from WKB theory that are readily calculable.

In the following tests, a test buoyancy profile was constructed using $n^2(z) = n^2_{\text{Munk}}(z) + f^2$, where $n_{\text{Munk}}(z) = n_0 e^{-z/B}$, and $n_0 = 3$ cph and B is a vertical scale length here assigned 1300 m. The Coriolis frequency was based on a latitude of 25°. This profile is shown in Fig. 3.

With the buoyancy profile specified, the other parameters found in the spectrum (Eq. 17) must be set. The computed values of $N_0 B$ and BE_{GM} are 6.67 $\text{m}\,\text{s}^{-1}$ and 8.32×10^{-2} vice the canonical values of 6.81 $\text{m}\,\text{s}^{-1}$ and 8.20×10^{-2}. The differences are due to numerical

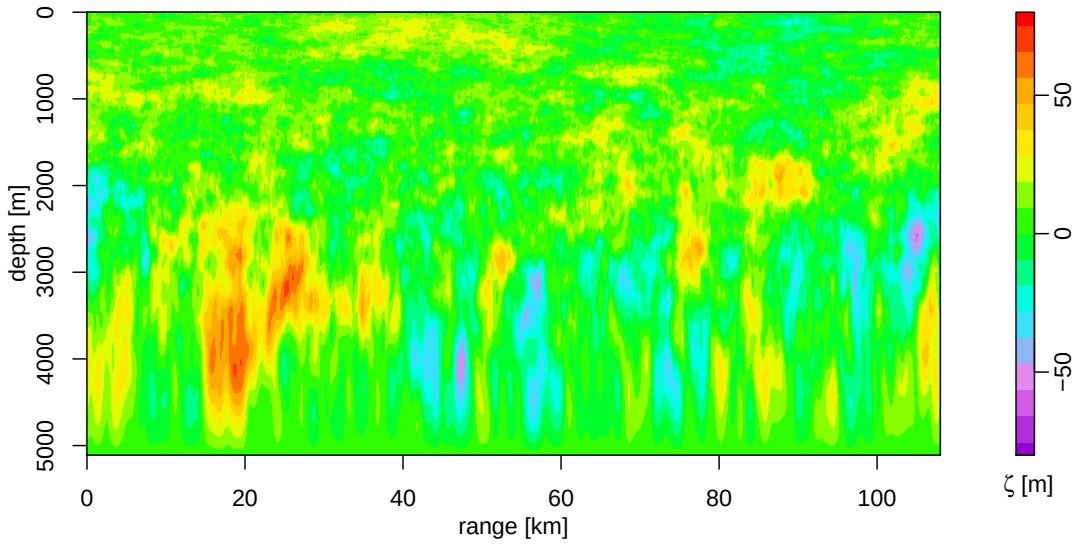

Figure 4: Color contour plot for a typical single realization of internal wave displacements. A range of 100 km is plotted (corresponding to an n/f aspect ratio of 20). `iseed` was -1 and `t` was 0.0.

error in the quadrature of $n(z)$. The low-mode cutoff was assigned the value of the canonical model, $j_* = 3$. The computational domain was 1000 km in range and 5.5 km in depth with sampling of 8192 points in the horizontal and 512 points in the vertical. In the program a base 2 FFT is used in the horizontal. This can be changed. A vertical sampling of 512 steps was chosen for convenience. This may be increased for larger j_*. The total number of internal wave vertical modes was chosen to be 80.

A portion of a typical realization is shown in Fig. 4. Note that because of the aspect ratio the contours are distorted. In reality the displacement contours form pancake-like structures stretched out in the horizontal.

VARIANCE

The simplest test is to estimate the displacement variance for a given depth and compare with WKB theory. The variance given by Munk [6] is

$$\langle \zeta^2 \rangle_{\text{WKB}} = \tfrac{1}{2} B E_{GM} \frac{n_0 B}{n(z)} \tag{20}$$

Multiplying both sides by $n(z)$ removes the depth dependence from the Munk variance, and one obtains

$$n(z) \langle \zeta^2 \rangle_{\text{WKB}} = \tfrac{1}{2} B E_{GM} n_0 B \tag{21}$$

which we compare to $n(z)\langle \zeta^2 \rangle$. The comparisons between Eq. 21 and the result from five

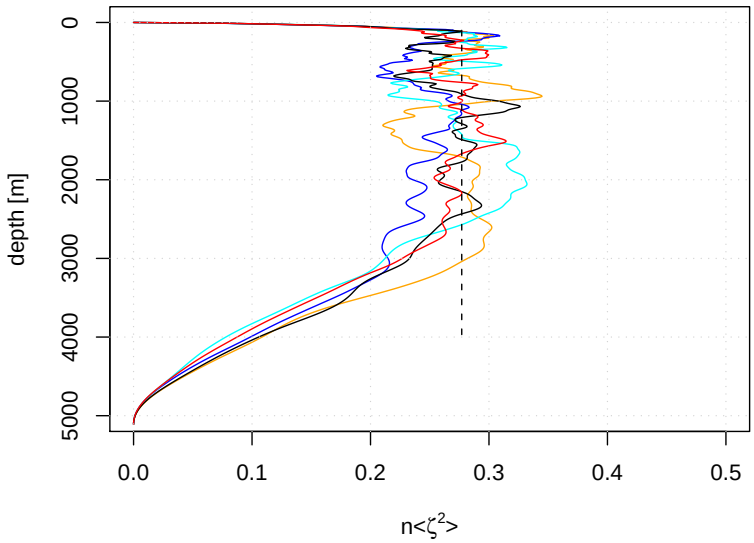

Figure 5: Five simulation realizations of $n\langle\zeta^2\rangle$ using `iseed` $= -1, -2, -3, -4, -5$. The vertical line is the WKB result at 0.277. This figure tests Eq. 21.

simulations are shown in Fig. 5. The simulations all used time `t` $= 0$, and random number generator seeds, `iseed`, of -1, -2, -3, -4, and -5. Over mid-depth, the simulated results are within $\pm$ 20% of the WKB prediction. The comparison above 2500 m is especially good. Very near the surface and toward the bottom, WKB is not expected to be valid.

TOWED DISPLACEMENT SPECTRA

We turn now to compare displacement spectra of (one-dimensional) horizontal wave number. Referred to as "towed," these spectra may be estimated from measurements using horizontal tows of sensors that are suspended at fixed depths from a ship steaming in one direction. The displacement may be inferred from temperature measurements, for example, by using the vertical temperature gradient and assuming a linear relationship.

From the simulations, we have the displacement data directly. A sample spectrum is shown in Fig. 6 from one of the simulations. There is considerable variability at low wave number. The theoretical spectrum can be obtained from Eq. 1 and is

$$TS_\zeta(k_x) = \int \sum_j \frac{S(\omega_{jk}, j) v_g}{\pi k} \varphi_{jk}^2(z)\, d|k_y| \tag{22}$$

Both spectra generally follow a k_x^{-2} dependence at high wave number. This is expected from WKB theory where for convenience, we obtain predictions by evaluating numerically an expression (Eq. 19) from Levine et al. [5]. This expression is complicated but may be

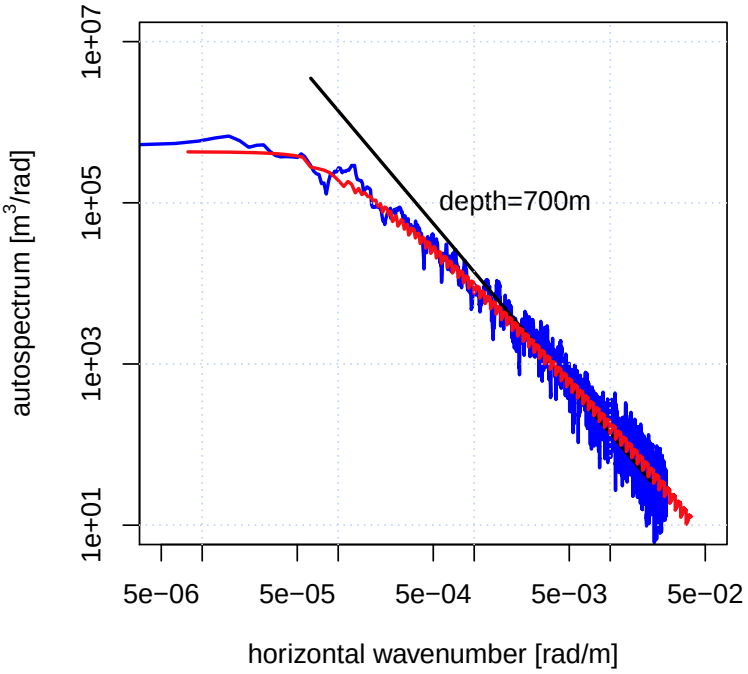

Figure 6: Comparisons of horizontal "towed" spectra at depth 700 m. A single realization is used (`iseed` $= -1$). The sample variance was 92.74. The autospectrum was estimated using the multitaper method with 8 tapers and a time-bandwidth product of 4. This is shown in blue. The estimated integral of the sample autospectrum was 93.77. The full theoretical expression (using 101 modes) is shown in red — this is Eq. 22. The discretization of the sampling in wave number space is evident as a "stair-step" appearance in the theoretical curve at higher wave numbers. The predicted variance based on an estimated integral of this curve is 83.97. Additionally, the Levine et al. [5] approximate expression is shown with a solid black line. This figure tests Eq. 22 and Eq. 23.

interpreted by considering the approximate formula given by Desaubies [1] for high wave number:

$$TS_\zeta(k_x) = \pi \left(\frac{2}{\pi}\right)^3 BE_{GM} \frac{j_* f}{n} \left(\ln \frac{n}{f} - \frac{n^2 - f^2}{2n^2}\right) k_x^{-2} \tag{23}$$

There is an $n(z)^{-1}$ dependence in depth and a k_x^{-2} dependence in wave number.

We expect from Fig. 5 that spectra near the surface and bottom will not follow the WKB behavior. We select a mid-depth of 700 m for the comparison. The sample spectrum is shown in Fig. 6 along with the WKB prediction. The model and data spectra are consistent

with each other and confirm the horizontal wave number behavior in the simulation.

Both the total variance and the horizontal spectral behavior of the simulations are consistent with the underlying model. Each simulation is an independent realization. The variability observed between simulations is typical for Monte Carlo experiments and demonstrates the acceptability of the method.

4 Summary

This report describes a numerical simulator for creating two-dimensional range/depth slices of sound speed variability associated with ocean internal waves. The simulator is both efficient and realistic. Designed for studies of internal wave effects on megameter acoustic propagation, it may also be used for short and intermediate ranges. The algorithm does not depend on WKB approximations, and therefore remains accurate in shallow water or near the ocean surface. Combined with the appropriate deterministic background profiles, the statistical model for the internal waves produces realizations that are true to ocean measurements while the method is easy to implement with low computational cost.

The method also can be extended to simulations wherein an accurate random wave field is needed for arbitrary values of x and y — i.e., fully 3-D simulations, not only simulations along a section $y = y_0$. In such cases, the tiling in the (k_x, k_y) domain should be square, so that dk_x and dk_y are the same everywhere. Gridding of the k_x and k_y axes then becomes uniform. Efficiency is retained as the contributions $\{k, dw_{jk}/dk, \varphi_{jk}(z)\}$ are assigned to be the contributions from the annulus for k' closest to the point (k_x, k_y).

References

[1] Desaubies, Y.J.F., Analytical representation of internal wave spectra, *J. Phys. Oceanogr.*, **6**, 976–981, 1976.

[2] Feynman, R.P., Forces in molecules, *Phys. Rev.*, **56**, 340, 1939.

[3] Hellmann, H., *Einführung in die Quantenchemie*, Franz Deuticke, Leipzig und Wien, 1937, p. 285.

[4] Henyey, F.S., D. Rouseff, J.M. Grochocinski, S.A. Reynolds, K.L. Williams, and T.E. Ewart, Effects of internal waves and turbulence on a horizontal aperture sonar, *IEEE J. Ocean. Eng.*, **22**, 270–279, 1997.

[5] Levine, M.D, J.D. Irish, T.E. Ewart, and S.A. Reynolds, Simultaneous spatial and temporal measurements of the internal wave field during MATE, *J. Geophys.. Res.*, **91**, 9709–9719, 1986.

[6] Munk, W.H., A survey of internal waves and small scale processes, in *Evolution of Physical Oceanography*, B.A. Warren and C. Wunsch, eds., Cambridge, MA, MIT Press, 1981.

[7] Winters, K.B., and E.A. D'Asaro, Direct simulation of internal wave energy transfer, *J. Phys. Oceanogr.*, **27**, 1937–1945, 1997.

Appendix: Pseudo-code

The pseudo-code for an implementation of the method (Fig. 7) and input parameters (Table 1) are given. Where appropriate, these parameters were used in the results described in this report.

```
loop over kh { kh = k0*r**m; m=0, 1, ..., nkh }
   compute modes, frequencies, and group velocities for each kh

   loop over kx { kx = 0, 1/Lx, ..., Nx/(2Lx)
      zero accumulator at kx and depth z
      compute d|ky|

      loop over j {1,2,...JMAX}
           compute variance Var = S(omega,j)*vgp/(pi*kh)*dj*dkx*d|ky|
           generate G+ from CN(0, Var)
           generate G- from CN(0, Var)

           loop over z
              accumulate [G+*e^(i*omega*t) + G-*e^(-i*omega*t)]*mode_j(z)
           endloop (z)
      endloop (j)
   endloop( kx )
endloop( kh )

loop over depth z
   zeta(z) = IDFT{ accumulant(kx;z) }
endloop (z)
```

Figure 7: Pseudo-code for a simulator.

Parameter	Description	Current Value	Pseudo-code
L_x	x-dimension (total range)	1×10^6 m	`Lx`
N_x	number of points in x-direction	8192	`Nx`
N_z	number of points in z-direction	512	
j_{max}	number of vertical displacement modes j	80	`JMAX`
t	evolution time for the realization	time [s]	`t`
N_k	number of horizontal wavenumber modes m	80	`nkh`
L_{kh0}	length of largest horizontal mode	1×10^5 m	2π/`k0`
`iseed`	initializes random number generator	integer (< 0)	
j_*	vertical displacement mode bandwidth	3	in `S()`
f	inertial frequency, $4\pi\Omega \sin$(latitude) [rad/s]	latitude dependent	in `S()`
Ω	rotation rate of Earth's surface	1 cycle/day	
BE_{GM}	strength [m]	8.32×10^{-2}	in `S()`
$n(z)$	buoyancy frequency profile [rad/s]	profile dependent	in `S()`
r	log-step increment, horizontal wavenumbers	$10^{0.04}$	`r`

Table 1: Parameters required in the algorithm.

REPORT DOCUMENTATION PAGE

Form Approved
OMB No. 0704-0188

PLEASE DO NOT RETURN YOUR FORM TO THE ABOVE ADDRESS.

1. REPORT DATE *(DD-MM-YYYY)*	2. REPORT TYPE	3. DATES COVERED *(From - To)*
11-03-2013	Technical Memorandum	

4. TITLE AND SUBTITLE

A Numerical Simulator of Ocean Internal Waves for Long-Range Acoustics

5a. CONTRACT NUMBER

5b. GRANT NUMBER
N00014-1-31-0009

5c. PROGRAM ELEMENT NUMBER

6. AUTHOR(S)

Frank S. Henyey and Stephen A. Reynolds

5d. PROJECT NUMBER

5e. TASK NUMBER

5f. WORK UNIT NUMBER

7. PERFORMING ORGANIZATION NAME(S) AND ADDRESS(ES)

Applied Physics Laboratory – University of Washington
1013 NE 40th Street
Seattle, WA 98105

8. PERFORMING ORGANIZATION REPORT NUMBER

APL-UW TM 1-13

9. SPONSORING/MONITORING AGENCY NAME(S) AND ADDRESS(ES)

Dr. Robert Headrick
Office of Naval Research, Code 32
875 North Randolph Street, Suite 4125
Arlington, VA 22203

10. SPONSOR/MONITOR'S ACRONYM(S)

11. SPONSOR/MONITOR'S REPORT NUMBER(S)

12. DISTRIBUTION/AVAILABILITY STATEMENT

Approved for public release; distribution is unlimited

13. SUPPLEMENTARY NOTES

14. ABSTRACT

In combination with an appropriate background ocean model, simulations of internal waves are necessary to create realistic scenarios for use in acoustic propagation studies. Our approach employs contemporary understanding of internal wave statistics with a simulator that produces two-dimensional (range/depth) slices of internal wave displacements. The method produces statistical realizations for acoustic studies that are true to ocean measurements with nominal computational cost.

15. SUBJECT TERMS

underwater sound propagation, numerical simulation, ocean internal waves, long-range acoustic propagation

16. SECURITY CLASSIFICATION OF:			17. LIMITATION OF ABSTRACT	18. NUMBER OF PAGES	19a. NAME OF RESPONSIBLE PERSON
a. REPORT	b. ABSTRACT	c. THIS PAGE			Rex K. Andrew
Uncl.	Uncl.	Uncl.	Unlimited	18	19b. TELEPHONE NUMBER *(Include area code)* 206 543 1250